LA-UR- 09-01621

Approved for public release; distribution is unlimited.

Title: Response of Alum Rock springs to the October 30, 2007 Alum Rock earthquake and implications for the origin of increased discharge after earthquakes

Author(s): Michael Manga (UC Berkeley)
Joel Rowland (LANL EES-14)

Intended for: Geofluids

Los Alamos
NATIONAL LABORATORY
EST. 1943

Response of Alum Rock springs to the October 30, 2007 Alum Rock earthquake and implications for the origin of increased discharge after earthquakes

Michael Manga[a,*] Joel C. Rowland [b]

[a]*Earth and Planetary Science, University of California, Berkeley*

[b]*Los Alamos National Laboratory, New Mexico, USA*

Abstract

The origin of increased stream flow and spring discharge following earthquakes have been the subject of controversy, in large part because there are many models to explain observations and few measurements suitable for distinguishing between hypotheses. On October 30, 2007 a magnitude 5.5 earthquake occurred near the Alum Rock springs, California, USA. Within a day we documented a several-fold increase in discharge. Over the following year, we have monitored a gradual return towards pre-earthquake properties, but for the largest springs there appears to be a permanent increase in the steady discharge at all the springs. The Alum Rock springs discharge waters that represent a mixture between modern ("shallow") meteoric water and old ("deep") connate waters expelled by regional transpression. After the earthquake, the increased discharge at the largest springs was accompanied by a small decrease in the fraction of connate water in the spring discharge. Combined with the rapid response, this implies that the increased discharge has a shallow origin. Increased discharge at these springs occurs for earthquakes that cause static volumetric expansion and those that cause contraction, supporting models in which dynamic strains are responsible for the subsurface changes that cause flow to increase. We show that models in which the permeability of the fracture system feeding the springs increases after the earthquake are in general consistent with the changes in discharge. The response of these springs to another earthquake will provide critical constraints on the changes that occur in the subsurface.

Key words: springs, permeability change, earthquake triggering, liquefaction

---

* Corresponding author

Email address: `manga@seismo.berkeley.edu` (Michael Manga).

1 Introduction

Increased discharge at springs following regional earthquakes is among the more interesting hydrological responses to earthquakes because the changes are often persistent, can be observed directly, and in some cases are large enough to be visually compelling. Despite a long history of documented changes, the origin of changes in discharge remains uncertain, and has been the subject of some scientific debate.

There are three general classes of explanations for increased discharge. First, coseismic static strain will increase pore pressure in the deformation quadrant that experiences compression (e.g., Wakita, 1975; Jonsson et al., 2003) leading to increased discharge at the surface (Muir-Wood and King, 1993). Second, dynamic strains created by the earthquake increase permeability permitting more rapid flow and hence increased discharge (e.g., Briggs, 1991; Rojstaczer and Wolf, 1992; Curry et al., 1994; Rojstaczer et al., 1995; Tokunaga, 1999; Sato et al., 2000; Wang et al., 2004a; Charmoille et al., 2005). The dynamic strain from distant earthquakes has been shown to at least temporarily increase permeability (e.g., Elkhoury et al., 2006). The breaching of hydraulic barriers or seals (e.g., Sibson, 1994; Brodsky et al., 2003; Wang et al., 2004b) is similar to the enhanced permeability model and the addition of a new water source should be reflected in changes in the composition or temperature of discharged fluids. Third, the origin of the excess water discharged after the earthquake lies in the shallowest subsurface where water is liberated by the consolidation or even liquefaction of near-surface unconsolidated materials (e.g., Manga, 2001; Manga et al., 2003; Montgomery et al., 2003).

Here we document the increased discharge and subsequent recovery of a set of thermal springs in San Jose, California, USA to the magnitude 5.5 October 30, 2007 Alum Rock earthquake. King et al. (1994) have previously reported the response of two of these springs to several regional earthquakes. Our monitoring extends this previous study to one more earthquake. More significantly, we sample water and measure discharge more frequently and consider the response of a greater number of springs. In section 2 we first describe the springs, their setting, and the sampling and measurement procedures. In section 3, we report measurements. In section 4 we characterize some of the attributes of earthquakes that have caused responses at the springs. We rule out mechanisms that appeal to coseismic volumetric strain and favor models in which the permeability of the fracture network feeding the springs increases after the earthquake. In section 5 we test proposed hypotheses and compare mathematical representations of conceptual models of hydraulic head and permeability increases with the observed changes. Finally, in section 6 we contrast the response of the stream into which the springs discharge with the observed changes at the springs.

2 Setting and properties of the springs

The Alum Rock complex of springs consists of a set of thermal springs that discharge from a fracture zone located updip of one strand of the Hayward fault. The springs lie along both sides of the topographic low created by Penitencia Creek. Figure 1 shows the location of the springs with respect to regional faults.

In a previous study of the hydrogeological and hydrogeochemical features of these springs, Rowland et al. (2008) noted significant compositional differences in the water from different springs. The discharged water was inferred to be a mixture of locally derived (but tritium free for at least spring AR 4) meteoric water and high chloride water with a pronounced oxygen isotope shift away from meteoric water. The high chloride water was interpreted to be old seawater (a connate water). Given the large variation over small spatial distances, Rowland et al. (2008) concluded that the flow paths feeding individual springs remain relatively isolated from each other. Figure 2 illustrates this conceptual model. Because the hydrogeochemistry at the spring outlets depends on the relative contribution of meteoric and connate water (hereafter also called "shallow" and "deep", respectively) any earthquake-induced changes in fault zone permeability or aquifer head should produce not only changes in discharge but potentially also hydrogeochemistry.

In the 1980s, King et al. (1994) documented flow and temperature changes at springs AR 4 and 11 following five regional earthquakes. In all cases flow increased, and for a couple earthquakes, a small decrease in temperature was recorded. No clear changes in electrical conductivity were recorded implying that there were no significant hydrogeochemical changes.

On October 30, 2007 at 8:05 pm local time, a magnitude 5.5 earthquake occurred along the Calaveras fault (http://earthquake.usgs.gov/). The following morning we collected water samples and made discharge measurements. We made subsequent measurements over the following year with a sampling frequency that decreased as the earthquake-induced changes decreased. Compared with King et al. (1994), we increased significantly the sampling frequency in order to document the evolution of the response; King et al. (1994) typically obtained only a single measurement of increased discharge after each earthquake. We also documented the responses of 12 springs and Penitencia Creek. Figure 3a shows the locations of these springs relative to each other and Penitencia Creek into which they discharge.

Springs discharge from outlets that range from seeps (AR 2, 5), to small pipes (AR 1, 6, 7, 8, 9,10 and 13) to large tunnels (springs 4, 11 and 12). Figure 3b shows some of these outlets. Discharge was measured by molding an oil-based modeling clay onto the rocks in order to capture all the spring water and focus it into a bucket for weighing or a graduated cyclinder for volume measurement. Uncertainties in discharge are estimated to be about 10%. Meaningful discharge measurements could only be made regularly at springs 4, 6, 11, 12 and 13. At other springs, there were multiple outlets or not enough head to gauge the flow. At some of the springs, water occasionally backed up to form pools which prevented discharge from being measured.

Temperature was measured with a thermocouple with accuracy of 0.2 ^{o}C until February 2008 and then with a thermistor with accuracy of 0.1 ^{o}C. O and H isotopes were measured with a GV IsoPrime gas source mass spectrometer, MultiPrep and elemental analyzer; analytical precision is better than 0.05 and 0.5 for δ^{18}O and δD, respectively. Chloride was measured in the lab with an ion specific electrode; uncertainties are estimated to be 10% and are dominated by uncertainty in the calibration and instrument drift between calibration measurements.

From 2003 until the time of the earthquake, we periodically measured discharge and temperature and collected samples for stable isotopes and major ion chemistry measurements. Up to 8 stable isotope samples were analyzed at the high discharge springs (4 and 11) while several of the seeps were only analyzed twice. The total number of pre-earthquake flow and temperature measurements varied similarly between springs. Rowland et al (2008) present the results of this monitoring program and discuss the implications of geochemical variations between springs on the connectivity of the fracture network feeding the springs.

3 Responses

At all spring outlets, discharge increased following the earthquake. Figure 4 shows the flow, temperature, and oxygen isotope response of the two largest springs, AR 4 and 11. These two springs are characterized by a nearly constant temperature ($\pm$0.7 and $\pm$1.5 ^{o}C, respectively). Flow increased by a factor of 3 and 3.5, respectively, within a day of the earthquake. Discharge declined gradually over the subsequent year, but more than 400 days after the earthquake is still above the pre-earthquake discharge: by about 35% for AR 4 and 20% for AR 11. For AR 11, the new steady discharge is similar to the steady discharge in the early 1980s (King et al., 1994) whereas pre-earthquake discharge was similar to that measured by King et al. (1994) in the early 1990s. At both springs there was a modest decrease in δ^{18}O, that occured soon after the earthquake (AR 4) or peaked a few months after the earthquake (AR 11), with a subsequent return to pre-earthquake values. We use δ^{18}O here to identify changes in water composition, rather than chloride, because we have more pre-earthquake measurements of the former and hence can more reliably compare responses with pre-earthquake values.

Measurements at the remaining three springs, AR 6, 12, and 13, for which reliable gauging measurements were made are shown in Figure 5. These springs differ from AR 4 and 11 in that they showed modest (a few degree) seasonal variations in temperature, presumably because their smaller discharge allows for more heat exchange with the shallow subsurface. The discharge responses at AR 12 and 13 are similar to those at the two largest springs, in that the largest discharges occured within the first few days after the earthquake, but differ in that discharge returned to the pre-earthquake values within a year. AR 6 is different. The first noticeable discharge at what was originally a minor seep appeared 3 days after the earthquake. Subsequently, discharge decreased and the spring returned to a seep within a few months. Measureable discharge returned during late spring 2008 – the rainy season – and again in December 2008. There is no clear change in δ^{18}O following the earthquake, but we emphasize that for AR 6 we have no pre-earthquake values and for AR 12 and 13 we have only 2 and 5 pre-earthquake values, respectively.

For the remaining springs, we are unable to obtain reliable or meaningful discharge measurements. AR 1, 2, 8 and 10 are either small seeps or part of a collection of small outlets. AR 5, 7 and 9 discharge from a flat region on the south side of the creek and spring water drains from a holding tank; the water from these two springs shows evidence of seasonal variations in composition that reflect seasonal precipitation or input of shallow groundwater. All these springs also show seasonal variations in temperature of several °C. We thus do not plot time series of our measurements. Instead we plot, in Figure 6, the relationship between O and H isotopic measurements and O isotopes and chloride concentration for all measurements and for all springs.

Figure 6 confirms that the water being discharged at the springs resembles a mixture of meteoric water (low chloride with O and H isotopes close to the meteoric water line) and a high chloride, O isotope shifted water that Rowland et al. (2008) inferred to be connate water. That all measurements generally lie along a line connecting these two endmembers supports the hypothesis that the discharged waters represent variable mixing between these two endmembers. Figure 6 shows that the modest decrease in δ^{18}O after the earthquake at AR 4 and 11, is accompanied by a decrease in chloride – consistent with a small shift towards the meteoric end member. The large variations in δ^{18}O and chloride at springs AR 5, 7 and 9 probably reflect enhanced discharge of shallow groundwater associated with seasonal precipitation.

The variations in δD are much larger than 8 times those in δ^{18}O implying that some other process besides mixing of the two end members causes their variation. There is no seasonal pattern in the variation of δD, nor is there a correlation with δ^{18}O. The Alum Rock springs actively degas H_2S. H_2S exchanges H with water and, because of the very large fractionation factors, the water will become enriched in the heavier isotope (e.g., Clark and Fritz, 1997). We speculate that time-variable interactions between H_2S gas and water lead to the observed variations in δD. As we do not have gas flux or composition measurements we do not attempt to quantify this hypothesis, but note that at the springs for which we have many pre-earthquake measurements (AR 4 and 11), there is no significant change in the variability of δD after the earthquake.

4 Features of the earthquakes that cause flow to increase

Table 1 lists the sign of the volumetric strain in the Penitencia Creek drainage basin generated by earthquakes that caused an increase in discharge. The list of responses include those in King et al. (1994), the response to the 2007 Alum Rock earthquake reported here, and a possible response to the 1906 San Francisco earthquake. For the latter we include a question mark in Table 1 because our reading of the Lawson (1908) report left us with some uncertainty about the actual springs being described, though increased discharge was widely reported throughout the area and to distances from the epicenter that exceed that of the Alum Rocks springs. For the 2007 earthquake, the volumetric strain was calculated by Kelly Grijalva using the deformation formulation in Pollitz (1996), the San Francisco area earth structure model of Dreger and Romanowicz (1994) and a slip model provide by Doug Dreger (personal communication). The springs lie close to a nodal plane in the pattern of volumetric strain, and peak strains are < 0.2 microstrain. As noted by King et al. (1994), discharge at Alum Rock springs increases for earthquakes that cause contraction, expansion, or little volumetric strain near the springs. Subsurface changes that increase flow are thus probably dominated by dynamic stresses.

Figure 7 shows the relationship between distance of the earthquake from the springs, earthquake magnitude, and the response. Earthquake locations and magnitudes are from the Northern California Earthquake Data Center. There is a clear magnitude-distance relationship for causing discharge to increase. However, we are unable to identify whether this is a true threshold because we do not have access to reliable measurements of the magnitude of increased discharge for events prior to the 2007 Alum Rock earthquake. That is, we cannot determine whether the magnitude of the discharge increase scales with the magnitude of earthquake-induced strains (for example peak ground velocity), as found for permeability changes in wells (Elkoury et al. 2006). Nevertheless we draw an empirical threshold separating earthquakes that have caused flow to increase from those that did not. For reference we include a second threshold obtained from a global compilation of streamflow changes (Wang et al. 2006). Over the cumulative period that was monitored, 1977-1991 and 2003-2008, there are no events clearly beyond this threshold line for which flow did not increase. Two earthquakes lie very close to the threshold (magnitude 4.8 events on January 15, 1981 and November 10, 1988); both caused contraction in the Alum Rock region. Because there were no earthquakes clearly beyond this line that did not cause a response, we cannot identify whether a repose time is needed for the springs to respond. The interval between earthquakes that caused a response is as short as 6.5 months so that if there is there is a repose or recovery time required for an earthquake-induced response it is less than half a year. A repose time of a couple years was identified for other earthquake triggered phenomena, including mud volcanoes in Azerbaijan (Mellors et al., 2007), Japan (Manga et al., 2009) or Italy (Bonini, 2009).

5 Discussion

We begin by listing features of the observations reported in the previous two sections that have bearing on the origins and implications of the spring response.

(1) Discharge increased at all springs.

(2) Peak discharges occur soon after the earthquake, within a few days.

(3) Discharge does not always return to pre-earthquake values, most notably at the two largest springs where we also have the best constraints on pre-earthquake discharges.

(4) For the largest springs there was no significant change in temperature, and we did not observe the small ($< 1^{\circ}$C) temperature decrease reported by King et al. (1994).

(5) Changes in δ^{18}O and chloride plot along a mixing line between meteoric and connate water end members (Figure 6) supporting the conceptual model (Figure 2) in which there are two sources of water that mix to varying degrees.

(6) While discharge increased by factors exceeding 3, the isotopic composition and chloride concentration changed modestly, if at all. For the two largest springs there is a small deviation towards the meteoric end-member composition. The observation of small if any change is consistent with the absence of any electrical conductivity changes reported by King et al. (1994) following previous earthquakes.

(7) There is a clear magnitude-distance relationship for earthquakes that induce responses (Figure 7).

(8) The response is dominated by dynamic rather than static stress changes (table 1).

Table 2 summarizes some of the predictions of proposed models for the increase in discharge after earthquakes. Features 1 and 6 support models in which permeability increases at shallow depths or within the fracture system feeding the springs; changes at depth would result in a delayed response. Feature 6 shows that we do not need to appeal to a new source of fluid or chemistry from a breached reservoir (e.g., Sibson, 1994; Wang et al., 2004b), a co- and post-seismic feature that has been documented at springs elsewhere (e.g., Yechieli and Bein, 2002; Stejskal et al., 2008). Given that there is no significant decrease in temperature at the springs that do not show seasonal variations in temperature (AR 4 and 11) and the discharged water at AR 4 contains no ^{3}H (Rowland et al., 2008), a source of water from the vadose zone (e.g., Manga et al., 2003) is highly unlikely (but see section 6 about the response of Penitencia Creek). Because of observation 6, we will next only consider models for changes in discharge, and address the changes of hydrogeochemistry qualitatively. Observation 8 is counter to predictions of the coseismic elastic strain model.

Figure 8 illustrates two conceptual models to explain the discharge change. We first consider the model in Figure 8a which appeals to an increase in permeability of the fracture systems feeding the springs. Second, we consider the model in Figure 8b in which an influx of fluid increases the head in the fracture system. We treat the fracture zone that delivers water to the spring as a homogenous one-dimensional aquifer. While clearly a great oversimplification of what must be a much more complex subsurface, similar (one-dimensional) models are commonly used to interpret postseismic responses to earthquakes (e.g., Rojstaczer et al., 1995; Roeloffs, 1998; Tokunaga, 1999; Sato et al. (2000); Manga, 2001; Manga et al., 2003; Montgomery et al., 2003; Wang et al., 2004ab) as well as to interpret discharge variations at springs (e.g., Manga, 1996). We will see that, while simple, the models will fit the observed changes is discharge extremely well.

5.1 Enhanced permeability model

Discharge Q from the fracture zone is governed by Darcy's equation

$$Q = -K_v A \frac{\partial h}{\partial z} \text{ at } z = 0, \tag{1}$$

where K_v is the vertical hydraulic conductivity of the fracture zone, A is the cross-sectional area across which fluid is being discharged, z is depth and h is hydraulic head. Equation (1) implies that the coseismic change in hydraulic conductivity is proportional to the coseismic change in discharge. We refer to a model in which hydraulic conductivity increases as the "enhanced permeability" model.

Subsequently, the increased discharge leads to a reduction of the head in the fracture system and a greater recharge from the surroundings. Approximating this latter flux as being proportional to the head difference between the far-field h_0 and that in the fracture system, the evolution of head in the fracture system can be approximated by the standard groundwater flow equation with an additional term that accounts for recharge to the fracture zone,

$$S_s \frac{\partial h}{\partial t} = K_v \frac{\partial^2 h}{\partial z^2} + \frac{K_h}{wD}(h_0 - h) \tag{2}$$

with boundary conditions

$$h = h_0 \text{ at } x = D \text{ and } \partial h/\partial z = 0 \text{ at } z = L. \tag{3}$$

Here S_s is the specific storage of the fracture zone, the width and depth of the fracture zone are w and L, respectively, and K_h is the horizontal conductivity of the region adjacent to the fracture zone. The horizontal aquifer extends to a distance $x = D$ where the head is fixed to h_0. The last term in equation (2) that describes recharge is a first order approximation. In this model we assume that storage properties, S, do not change, though both hydraulic conductivity and storage properties can be influenced by earthquakes (e.g., Jang et al., 2008).

The steady state head distribution in the fracture zone is

$$h = h_0 \left(1 - \frac{\sinh(\mu z) + \sinh[\mu(2L - z)]}{\sinh(2\mu L)} \right) \tag{4}$$

where $\mu = \sqrt{K_h / K_v D w}$. The corresponding steady state discharge is

$$Q_0 = K_v A \mu h_0 \left[\frac{1 - \cosh(2\mu L)}{\sinh(2\mu L)} \right]. \tag{5}$$

Following the earthquake, we assume that K_v increases by an amount linearly proportional to the increase in discharge. The subsequent evolution of discharge can be obtained by solving the time-dependent diffusion equation (2) with a new hydraulic conductivity K_{v_f} and an initial condition equal to the difference between the steady state solution with the initial conductivity (now denoted K_{v_i}) and final conductivity K_{v_f}. The solution can be obtained by adapting that for an analogous problem in section 4.14 of Carslaw and Jaeger (1959). The evolution of head is then given by

$$\begin{aligned} h(z,t) = h_0 & \left[1 - \frac{\sinh(\mu_f z) + \sinh[\mu_f(2L - z)]}{\sinh(2\mu_f L)} \right] - \\ & \frac{16 h_0 L^2}{\pi} e^{-K_h t / D w S_s} \sum_{n=1}^{\infty} \left[\frac{\mu_i^2}{(2n-1)^2 \pi^2 + 4L^2 \mu_i^2} - \frac{\mu_f^2}{(2n-1)^2 \pi^2 + 4L^2 \mu_f^2} \right] \\ & \times \frac{1}{(2n-1)} \sin \left[\frac{(2n-1)\pi z}{2L} \right] e^{-(2n-1)^2 \pi^2 K_{v_f} t / 4 S_s L^2} \end{aligned} \tag{6}$$

where the subscripts i and f indicate values before (initial) and after (final) the earthquake. The corresponding discharge can be obtained by evaluating Darcy's equation (1) at $z = 0$,

$$Q(t) = -K_{v_f} A \mu_f h_0 \frac{[1 - \cosh(2\mu_f L)]}{\sinh(2\mu_f L)} + 8K_{v_f} A h_0 L e^{-K_h t/DwS_s} \sum_{n=1}^{\infty} \left[\frac{\mu_i^2}{(2n-1)^2\pi^2 + 4L^2\mu_i^2} - \frac{\mu_f^2}{(2n-1)^2\pi^2 + 4L^2\mu_f^2} \right] e^{-(2n-1)^2\pi^2 K_{v_f} t/4S_s L^2} \tag{7}$$

This model is similar to that used by Rojstaczer et al. (1995) and later invoked by Sato et al. (2000) and Tokunaga (1999) to explain changes in discharge. It differs in that it accounts for the increased recharge to the fracture system following its reduction in head, the last term in equation (2).

This enhanced permeability model is characterized by 4 parameters

$$\alpha = \frac{K_{v_f} A h_0}{L}; \quad R = \frac{K_{v_f}}{K_{v_i}}; \quad \nu = \frac{K_h}{DwS_s}; \quad T = \sqrt{\frac{\nu L^2 S_s}{K_{v_f}}} \tag{8}$$

The first, α, is a scaling parameter for the magnitude of discharge. The second, R, is the ratio of fracture zone conductivity after and before the earthquake. R can be determining directly from the measured increased in discharge. Third, ν, is an inverse hydraulic diffusion time scale. The fourth, T is the ratio of vertical to horizontal flow time scales. With these parameters, equation (7) can be written

$$Q(t) = -\alpha T \frac{[1 - \cosh 2T]}{\sinh 2T} + 8\alpha e^{-\nu t} \sum_{n=1}^{\infty} \left[\frac{RT^2}{(2n-1)^2\pi^2 + 4RT^2} - \frac{T^2}{(2n-1)^2\pi^2 + 4T^2} \right] e^{-(2n-1)^2\pi^2 \nu t/4T^2} \tag{9}$$

The ratio of final post-earthquake steady-state discharge Q_f to the pre-earthquake discharge Q_0 is

$$\frac{Q_f}{Q_0} = \sqrt{R} \frac{\sinh(2\sqrt{R}T)}{\sinh(2T)} \left(\frac{1 - \cosh 2T}{1 - \cosh 2\sqrt{R}T} \right) \tag{10}$$

From equation (10) we can see that for small T, $Q_f/Q_0 \to 1$, whereas for large T, $Q_f/Q_0 \to \sqrt{R}$. Thus, the initial response to a conductivity increase is an increase in discharge by a factor of R, and the final steady discharge is increased by a factor $\leq \sqrt{R}$.

5.2 Increased head model

If K_v remains unchanged by the earthquake, and assuming A does not change, Darcy's law (1) requires that head gradients, and hence head, changed. Increased stream discharge owing to increased hydraulic heads have been proposed to result from consolidation (e.g., Manga et al., 2003), breaching barriers to release pressurized water (Wang et al., 2004b) or by increasing permeability perpendicular to the fracture system so that the fracture zone is rapidly recharged (Wang et al., 2004a).

Here we follow the formulation in Wang et al. (2004a) and allow a pulse of recharge to the fracture system over the depth interval $z = L'$ to $z = L$. The groundwater flow equation for this problem can be written as

$$S_s \frac{\partial h}{\partial t} = K_v \frac{\partial^2 h}{\partial z^2} + F \tag{11}$$

where F is the rate of recharge to the fracture zone per unit volume. At the time of the earthquake we let $F = F_0 \delta$ over the depth interval $L' < z < L$, where $\delta = 1$ at $t = 0$ and $\delta = 0$ for $t > 0$. The solution for discharge is given by (e.g., Wang et al., 2004)

$$Q(t) = Q_0 + \frac{2K_v A F_0}{S_s L} \sum_{n=1}^{\infty} (-1)^{n-1} \sin\left[\frac{(2n-1)^2 \pi^2 (L - L')}{2L}\right] \times e^{-(2n-1)^2 \pi^2 K_v t / 4 S_s L^2} \tag{12}$$

This model is characterized by 4 parameters

$$Q_0; \quad \beta = \frac{2K_v A F_0}{S_s L}; \quad \Lambda = \frac{K_v}{S_s L^2}; \quad (L - L')/L. \tag{13}$$

Of these, the discharge Q_0 prior to the earthquake is known. We will fix $(L - L')/L$ to 1 in order to reduce the number of parameters. This choice is consistent with the very rapid increase in discharge – as $(L - L')/L$ decreases, the time between the earthquake and the peak postseismic discharge increases. Previous studies that documented peak responses within days inferred $(L - L')/L$ close to 1 (Manga et al., 2003; Wang et al., 2004) and these studies guide our simplification.

5.3 Application of models to the flow observations

We determined model parameters and their uncertainties by fitting equations (9) and (12) to the discharge measurements using gnuplot (http://www.gnuplot.info/).

Figure 9 compares data for AR 4, 6, 11, 12, and 13 with best-fit models. Tables 3 and 4 list the models parameters. The larger uncertainties in the parameters of the enhanced permeability model (table 3) compared to the head increase model (table 4) reflects the larger number of fitted parameters (3 compared with 2, respectively) and the trade-offs between their values.

In general, the enhanced permeability model, equation (9), captures the recovery of the discharge after the earthquake. Importantly, this model can also explain the permanent change in discharge measured at springs AR 4 and 11. The magnitude of the permanent change in discharge depends on the conductivity change R and ratio of time scales T – equation (10). The increased head model also captures the postseismic increase and subsequent decrease of discharge, but requires a return to pre-earthquake discharge Q_0. The values of ν and T for the permeability enhancement model, or Λ in the increased head model, correspond to reasonable hydraulic diffusivities of $O(10^{-1})$ m^2/s (e.g. Roeloffs, 1996) if we assume a length scale L of 1 km.

Given the small changes in water hydrogeochemistry at the largest springs we do not attempt to quantitatively apply the models in Figure 8 to the data. We note, however, that the essentially constant water composition may imply a long residence time of water in the fracture system compared to the period over which discharge changes. Otherwise the water entering the fracture system in both cases should show up as a dilution of the chloride concentration and decrease in δ^{18}O. Whereas discharge increased by a factor of 3-7 for the springs shown in Figures 4 and 5, the water is diluted by at most by a few percent by the shallow meteoric end member. For the enhanced permeability model (Figure 8a), springs AR 4 and 11 have the largest value of T – the springs for which horizontal flow times are shortest relative to vertical flow times – and also show the most pronounced dilution of discharged water, as expected. Finally, if the fracture system was draining water from two distinct regions, an increase in fracture zone permeability would increase the proportion of water being recharged from the deeper region, presumably our chloride-rich end-member. If the enhanced permeability model is in fact a good description of the subsurface, then the shallow and deep water must mix upgradient and before the mixture is drawn in the fracture system where the permeability was increased.

We do not consider quantitatively models in which the decrease of post-seismic discharge occurs because of a gradual sealing of flow paths and hence a decreasing permeability (e.g., Gratier, 2003; Claesson et al., 2004, 2007). We simply note that if the flow changes are dominated by the sealing of opened flow paths or reduction of earthquake-enhanced permeability, that the final permeability at AR 4 and 11 must be different from the pre-earthquake value (feature 3 above).

6 Response of Penitencia Creek

Penitencia Creek also responded to the earthquake by increasing its discharge. The Santa Clara water district maintains a gauge about 4 km downstream of the springs, formerly USGS station 11172100. Measurements 8 and 16 hours after the earthquake show an approximate doubling of the discharge from about 4 to 8 l/s. Figure 10 shows that the increased discharge persists for at least 12 days until rainfall on November 11 adds ambiguity to interpreting subsequent discharge measurements. Uncertainity in discharge, based on the accuracy of the water level gauge, is about 10%. The increase in discharge is much greater than the total discharge at the Alum Rock springs (less than 2 l/s on October 31, 2007) implying a source for some of the excess discharge other than the springs. As with the springs, the peak increased discharge occurred within a couple days of the earthquake.

We did not collect water from Penitencia Creek until November 5, 2007. Water samples from the creek were collected upstream of all the springs. The sample from November 5 is unusual compared to all the other creek samples collected both before, and since, in two respects shown in figure 11. First, its O and H isotopic composition falls off the trend defined by the other water samples. Second, the chloride concentration is the highest of any of the creek samples. One explanation for the chloride enrichment and isotope shift is that the water in the stream experienced significant evaporation and transpiration in the vadose zone prior to entering the stream. A chloride enrichment of about 50% over typical values for stream water would imply that 1/3 of the original water was lost relative to typical streamwater. In an atmosphere with 20% humidity, evaporation of 10% of the water would have imparted a shift in O and H that would bring the original water close to a line described by other streamflow samples (we use the fractionation factors of Cappa et al. (2003) at 20 ^{o}C at 20.4% humidity in this representative calculation). The remaining water loss to account for the 50% enrichment in chloride could be lost by transpiration as water uptake by roots imparts no fractionation (Gat, 1996). November 5, 2007 was near the end of the dry season and before any significant rainfall so soil water should have experienced significant evapotranspiration. In fact, most of the water samples from the dry season lie on a trend that deviates from the meteoric water line by having a more shallow slope, but none deviate as much as the Novemer 5, 2007 sample. We suggest that shaking by the earthquake liberated this water, perhaps by consolidating loose materials (Manga et al., 2003), and that this water entered the stream. Unfortunately, as no water samples from the creek were collected during the first 5 days after the earthquake, we must view this hydrogeochemically-based inference as highly speculative as it is based on a single measurement.

The recession of stream discharge after the earthquake offers an additional opportunity to distinguish between explanations for the increased discharge.

During periods without significant precipitation, discharge Q will decrease approximately exponentially with time t,

$$Q(t) \propto e^{-\alpha t}. \tag{14}$$

The recession constant α is proportional to the permeability of the aquifers providing baseflow. For the recession from October 14-19 following the storm on October 13, $\alpha = 0.105 \pm 0.005$ day^{-1}; for the period after the earthquake, November 1-5, $\alpha = 0.078 \pm 0.026$ day^{-1}; following the storm on November 11, $\alpha = 0.077 \pm 0.022$ day^{-1} for the period November 12-15. There is no clear change in recession characteristics, consistent with models in which the earthquake increases head in the aquifers providing baseflow (e.g., Manga, 2001; Manga et al., 2003; Wang et al., 2004a). However, we once again emphasize the limited time interval over which the effect of the earthquake can be seen before precipitation obscures the response. In addition a small reservoir (1.2×10^5 m^3 capacity) in the upper reaches of the Penitencia Creek drainage has an unknown, but likely very small, effect on the discharge at the gauge.

7 Conclusions

The Alum Rock springs all showed a rapid increase in discharge followed by a gradual recovery. The large change in discharge was accompanied by either small or no significant changes in water composition. The shift towards a composition more similar to meteoric water and the rapid response imply that the excess water originates from shallow depths and that changes occur close to the surface. This does not mean that deep changes do not occur, simply that deep changes do not dominate the observed responses. The lack of correlation between increased discharge and the sign of volumetric strain favors a response induced by dynamic strain.

We briefly considered two different models to explain the flow changes. We favor the model in which permeability increased in the fracture zone feeding the springs over a model in which fluid pressures increased because of the permanent (over a 1 year time window) change in the steady discharge – a feature that requires a permanent change in properties or boundary conditions. Nevertheless, the head increase model also fits the data quite well. There is a third possibility, we did not consider, that permeability increased after the earthquake, and the subsequent recovery is governed by a gradual decrease in permeability.

We should ultimately be able to distinguish between the three models for the evolution of discharge by documenting the response to yet another earthquake. In particular, the recession characteristics of discharge depend on the permeability change for the enhanced permeability model in Figure 8a. Recession will be identical for all earthquakes for the head-change model in Figure 8b (Manga, 2001), that is, Λ will be the same. If the response to a subsequent earthquake shows a different recession parameter (different Λ), and a recession that does not scale with the permeability increase as described in equation (9), we would favor recession being dominated by time-evolving reduction of permeability. Unfortunately, the long interval between flow measurements made by King et al. (1994) prevents us from performing these tests retrospectively. And, unlike streams where we can use baseflow recession before and after earthquakes to identify changes (e.g., Manga, 2001; Montgomery et al., 2003), because the normal state of the springs is a steady discharge, we have (so far) only a single recession event to probe the subsurface changes.

Acknowledgments: We thank Alum Rock Park for providing sampling permits; NSF for support to respond to the earthquake, NASA for support in making measurements prior to the earthquake, and the Miller Institute for Basic Research in Science for supporting the analysis presented here; the many colleagues, students and in particular family members who assisted with sampling; Tim Rose for ideas and geochemical analyses; Wenbo Yang for the O and H isotope measurements; Linda Kalnejas for help with ion chromatography measurements; Kelly Grivalja for calculating strain; the Santa Clara water district and staff for maintaining the Penitencia Creek gauge and making corrected data available; Chi Wang for discussions and suggestions.

References cited

Andrews DJ, Oppenheimer DH, Lienkamper JJ (1993) The missing link between the Hayward and Calaveras faults. *Journal of Geophysical Research* **98**, 12,083-12,095.

Bonini M (2009) Mud volcano eruptions and earthquakes in the Apennines, Italy. *Tectonophysics* in review.

Briggs RO (1991) Effects of Loma Prieta earthquake on surface water in Waddell Valley. *Water Resources Bulletin* **27**, 991-999.

Brodsky EE, Roeloffs E, Woodcock D, Gall I, Manga M (2003) A mechanism for sustained ground water pressure changes induced by distant earthquakes. *Journal of Geophysical Research* **108**, doi:10.1029/2002JB002321.

Cappa CD, Hendricks MB, DePaolo, DJ, Cohen RC (2003) Isotopic fractionation of water during evaporation. *Journal of Geophysical Research* **108**, 4525, doi:10.1029/2003JD003597.

Carslaw HS, Jaeger JC (1959) Conduction of heat in solids, 2nd edition, Oxford University Press.

Charmoille A, Fabbri O, Mudry J, Guglielmi Y, Bertrand C (2005) Post-seismic permeability change in a shallow fractured aquifer following a M-L

5.1 earthquake (Fourbanne karst aquifer, Jura outermost thrust unit, eastern France). *Geophysical Research Letters* **32**, L18406, doi:10.1029/2005GL023859.

Claesson L, Skelton A, Graham C, Dietl C, Morth M, Torssander P, Kockum I (2004) Hydrogeochemical changes before and after a major earthquake. *Geology* **32**, 641-644.

Claesson L, Skelton A, Graham C, Morth CM (2007) The timescale and mechanisms of fault sealing and water-rock interaction after an earthquake. *Geofluids* **7**, 427-440.

Clark ID, Fritz O (1997) Environmental isotopes in hydrogeology, CRC Press, 352 pages.

Curry RR, Emery BA, Kidwell TG (1994) Sources and magnitudes of increased streamflow in the Santa Cruz Mountains for the 1990 water year after the earthquake, in *US Geological Survey Professional Paper 1551E*, 31-50.

Dreger D, Romanowicz B (1994), Source characteristics of events in the San Francisco Bay Region. *U. S. Geological Survey Open File Report 94-176*, 301-309.

Elkhoury JE, Brodsky EE, Agnew DC (2006) Seismic waves increase permeability. *Nature* **441**, 1135-1138.

Gat JR (1996) Oxygen and hydrogen isotopes in the hydrologic cycle. *Annual Reviews of Earth and Planetary Science* **24**, 225-262.

Gratier JP, Favreau P, Renard F (2003) Modeling fluid transfer along California faults when integrating pressure solution crack sealing and compaction processes. *Journal of Geophysical Research* **108**, 2104.

Jang CS, Liu CW, Chia Y, Cheng LH, Chen YC (2008) Changes in hydrogeological properties of the River Choushui allunvial fan aquifer due to the 1999 Chi-Chi earthquake, Taiwan. *Hydrogeology Journal* **16**, 389-397.

Jonsson S, Segall P, Pedersen R, Bjornsson G (2003) Post-earthquake ground movements correlated to pore-pressure transients. *Nature* **424**, 179-183.

King C-Y, Basler D, Presser TS, Evans WC, White LD, Minissale A (1994) In Search of Earthquake-Related Hydrologic and Chemical-Changes Along Hayward Fault. *Applied Geochemistry* **9**, 83-91.

Lawson AC (1908) The California Earthquake of April 18, 1906. Report of the state earthquake investigation commission, Carnegie Institution of Washington, Washington, D.C., vol. 1.

Manga M (1996) Hydrology of spring-dominated streams in the Oregon Cascades. *Water Resources Research* **32**, 2435-2439.

Manga M (2001) Origin of postseismic streamflow changes inferred from baseflow recession and magnitude-distance relations. *Geophysical Research Letters*

28, 2133-2136.

Manga M, Brodsky EE, Boone M (2003) Response of streamflow to multiple earthquakes and implications for the origin of postseismic discharge changes. *Geophysical Research Letters* **30**, doi:10.1029/2002GL016618.

Manga M, Brumm M, Rudolph (2009) Earthquake triggering of mud volcanos: A review. *Marine and Petroleum Geology* in press.

Mellors R, Kilb D, Aliyev A, Gasanov A, Yetirmishli G (2007) Correlations between earthquakes and large mud volcano eruptions. *Journal of Geophysical Research* **112**, B034304, doi:101029/2006JB004489.

Montgomery DR, Manga M (2003) Streamflow and water well responses to earthquakes. *Science* **300**, 2047-2049.

Montgomery DR, Greenberg HM, Smith DT (2003) Streamflow response to the Nisqually earthquake. *Earth and Planetary Science Letters* **209**, 19-28.

Muir-Wood R, King GCP (1993) Hydrological signatures of earthquake strain. *Journal of Geophysical Research* **98**, 22,035-22,068.

Pollitz FF (1996) Coseismic deformation from earthquake faulting on a layered spherical earth. *Geophysical Journal International* **125**, 1-14.

Roeloffs EA (1996) Poroelastic techniques in the study of earthquake-related hydrologic phenomena. *Advances in Geophysics* **37**, 135-195.

Roeloffs EA (1998) Persistent water level changes in a well near Parkfield, California, due to local and distant earthquakes. *Journal of Geophysical Research* **103** 869-889.

Rojstaczer S, Wolf S (1992) Permeability changes associated with large earthquakes: An example from Loma Prieta, California. *Geology* **20**, 211-214.

Rojstaczer S, Wolf S, Michel R (1995) Permeability enhancement in the shallow crust as a cause of earthquake-induced hydrological changes. *Nature* **373**, 237-239.

Rowland JC, Manga M, Rose TP (2008) The influence of poorly interconnected fault zone flow paths on spring geochemistry. *Geofluids* **8**, 93-101.

Sato T, Sakai R, Furuya K, Kodama T (2000) Coseismic spring flow changes associated with the 1995 Kobe earthquake. *Geophysical Research Letters* **27**, 1219-1222.

Sibson RH (1994) Crustal stress, faulting and fluid flow. *Geological Society of London, Special Publication* **78**, 69-84.

Stejskal V, Malek J, Novotny O (2008) Variations in discharge and temperature of mineral springs at the Frantiskovy Lazne Spa, Czech Republic, duing a nearby earthquake swarm. *Studia Geophysica eet Geodaetica* **52**, 589-606.

Tokunaga T (1999) Modeling of earthquake-indiced hydrological changes and possible permeability enhancement due to 17 January 1995 Kobe earthquake, Japan. *Journal of Hydrology* **223**, 221-229.

Wakita H (1975) Water wells as possible indicators of tectonic strain. *Science* **189**, 553-555.

Wang C-Y, Wang C-H, Manga M (2004a) Coseismic release of water from mountains: Evidence from the 1999 (Mw = 7.5) Chi-Chi, Taiwan, earthquake. *Geology* **32**, 769-772.

Wang C-Y, Dreger D, Manga D, Wong A (2004b) Streamflow increase due to rupturing of hydrothermal reservoirs: Evidence from the 2003 San Simeon, California, earthquake. *Geophysical Research Letters* **31**, L10502, doi:10.1029/2004GL020124.

Wang C-Y, Wong A, Dreger DS, Manga M(2006) Liquefaction Limit during Earthquakes and Underground Explosions: Implications on Ground-Motion Attenuation. *Bulletin Seismological Society America* **96**, 355-363.

Yechieli Y, Bein A (2002) Response of groundwater systems in the Dead Sea Rift Valley to the Nuweiba earthquake: Changes in head, water chemistry, and near-surface effects. *Journal of Geophysical Research* **107**, 2332, doi:10.1029/2001JB001100.

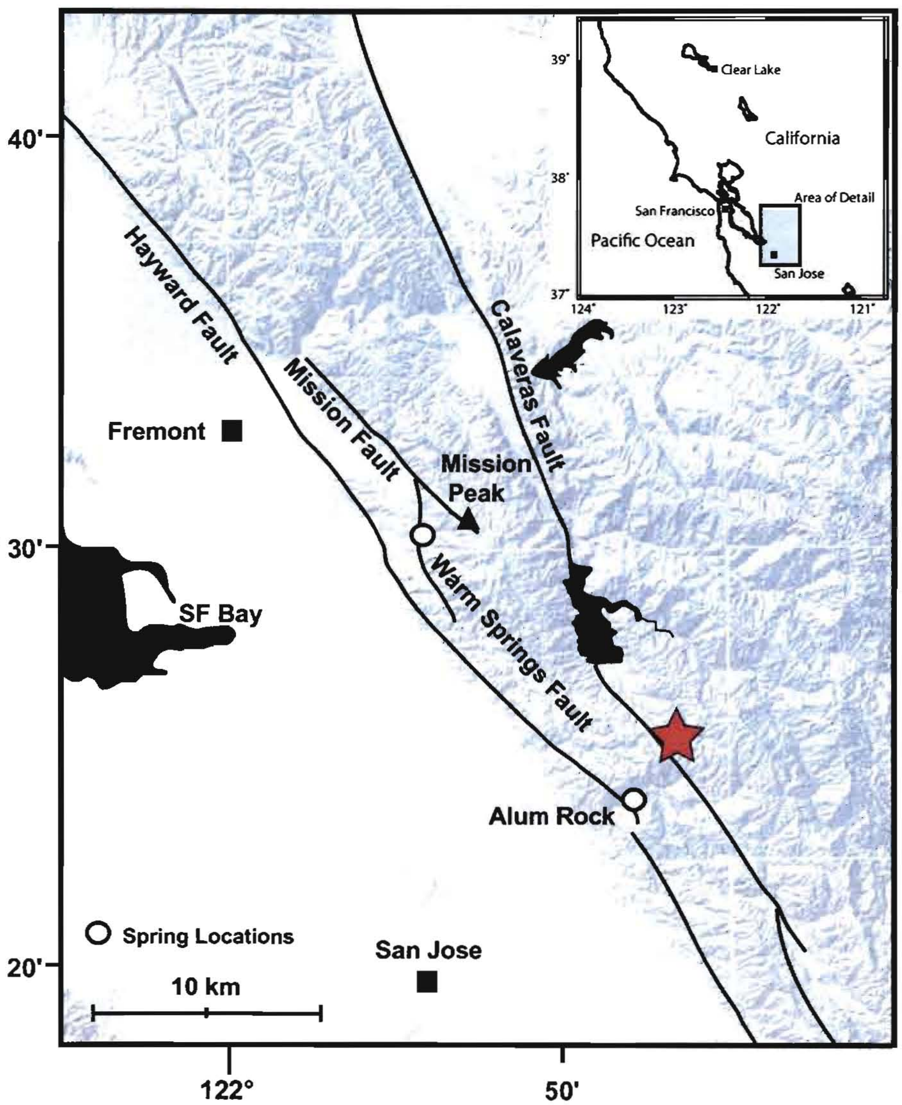

Fig. 1. Location of Alum Rock springs, the 30 October 2007 magnitude 5.5 Alum Rock earthquake (star), and regional faults. Background is the US Geological Survey 10 m DEM. Fault locations are from Andrews et al. (1993).

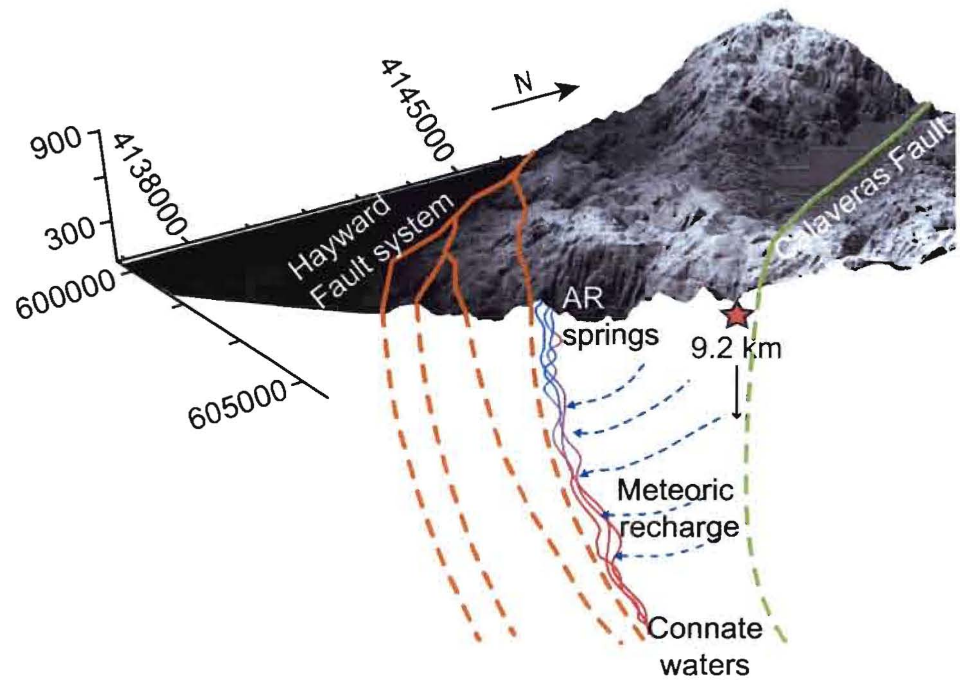

Fig. 2. Conceptual model showing the relationship between faults, flow paths and the sources of deep connate waters and shallow groundwater that has a modern meteoric origin. Location of the Alum Rock earthquake is shown with the star.

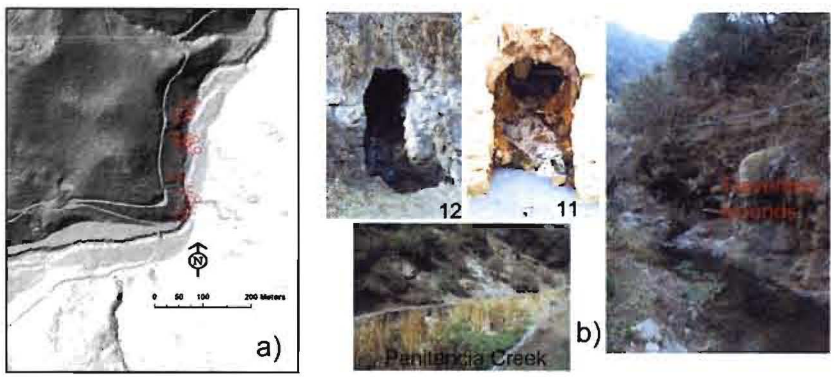

Fig. 3. a) Location of springs along Penitencia Creek. Numbers correspond to spring numbers. DEM source: GeoEarthScope, Northern California LiDAR funded by NSF. b) Photographs of spring 12 and, which emerge from tunnels, Penitencia Creek, and travertine mounds which form at the spring outlets.

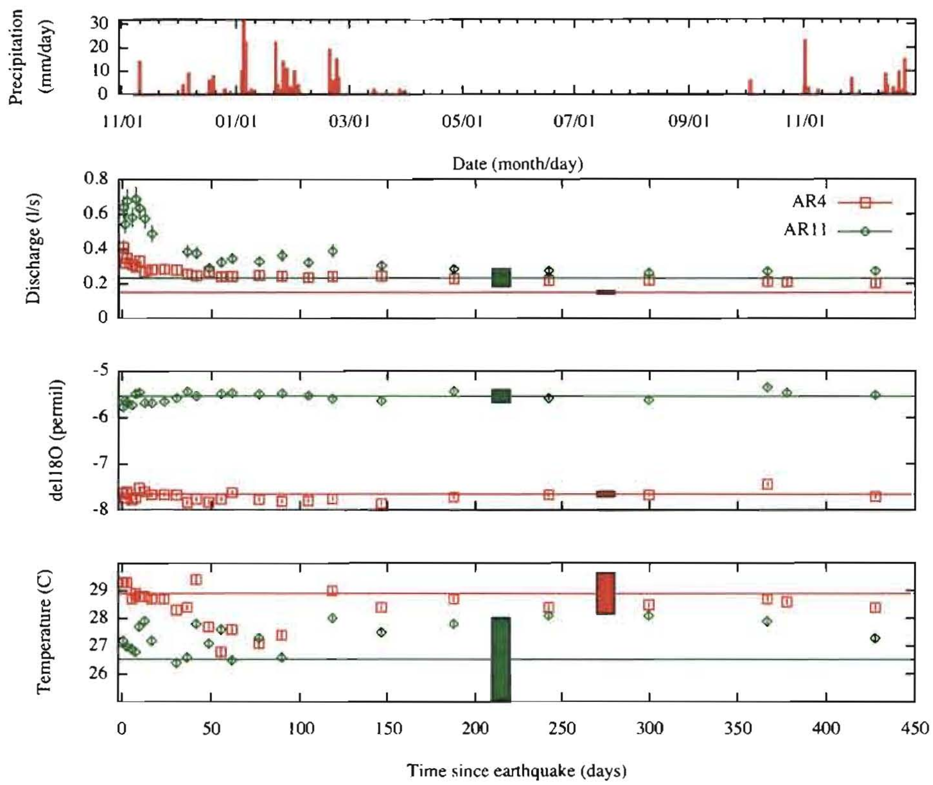

Fig. 4. Discharge, $\delta^{18}O$, and temperature responses at the two largest springs, AR 4 and 11, as a function of time in days since the October 30, 2007 Alum Rock earthquake. Histograms at the top shows precipitation in mm/day. Horizontal lines are pre-earthquake values and the boxes the standard deviations of pre-earthquake measurements.

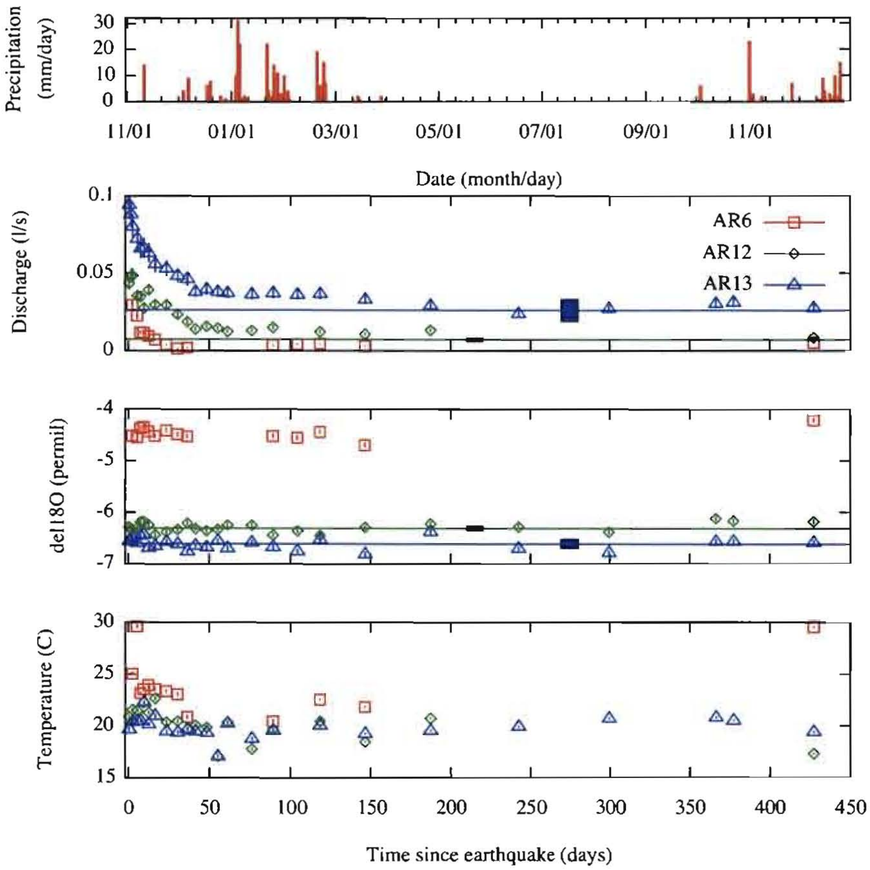

Fig. 5. Discharge, $\delta^{18}O$, and temperature responses at springs AR 6, 12, and 13 as a function of time in days since the October 30, 2007 Alum Rock earthquake. Histograms at the top shows precipitation in mm/day. Horizontal lines are pre-earthquake values and the boxes the standard deviations of pre-earthquake measurements. Pre-earthquake oxygen isotope values are not known for AR 6 which was a minor seeps prior to the earthquake.

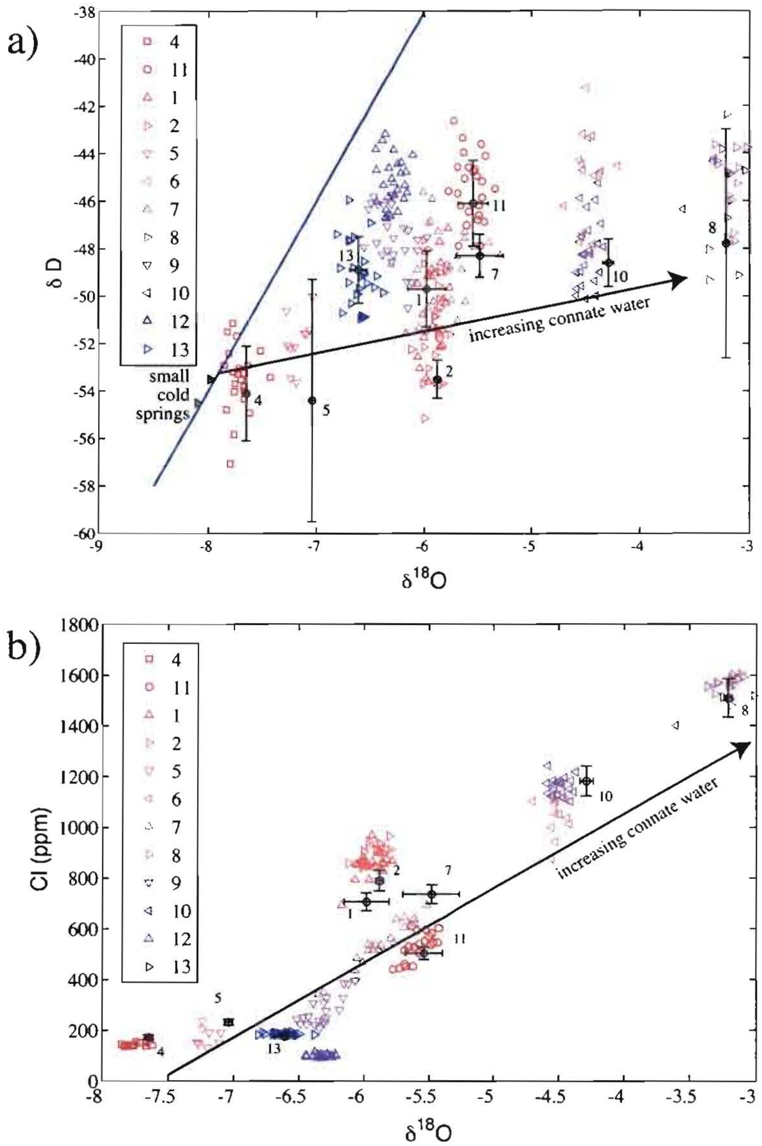

Fig. 6. Relationship between a) δ^{18}O and δD and b) δ^{18}O and chloride for springs waters collected after the Alum Rock earthquake (colored symbols) and pre-earthquake volaues (black circles). Error bars on pre-earthquake values reflect the variability in the measurements, summarized and reported by Rowland et al. (2008). Uncertainities on any individual measurement are 0.05 permil for δ^{18}O, 0.5 permil for δD, and 10% for chloride. Error bars are not shown for colored symbols. The two filled black triangles in a) are water samples from small springs at high elevations in the drainage basin and the sloping black line is the global meteoric water line $\delta D = 8\delta^{18}O + 10$. There is a pronounced oxygen isotope shift in the spring waters, and b) shows that this isotope shift is correlated with an enrichment in chloride.

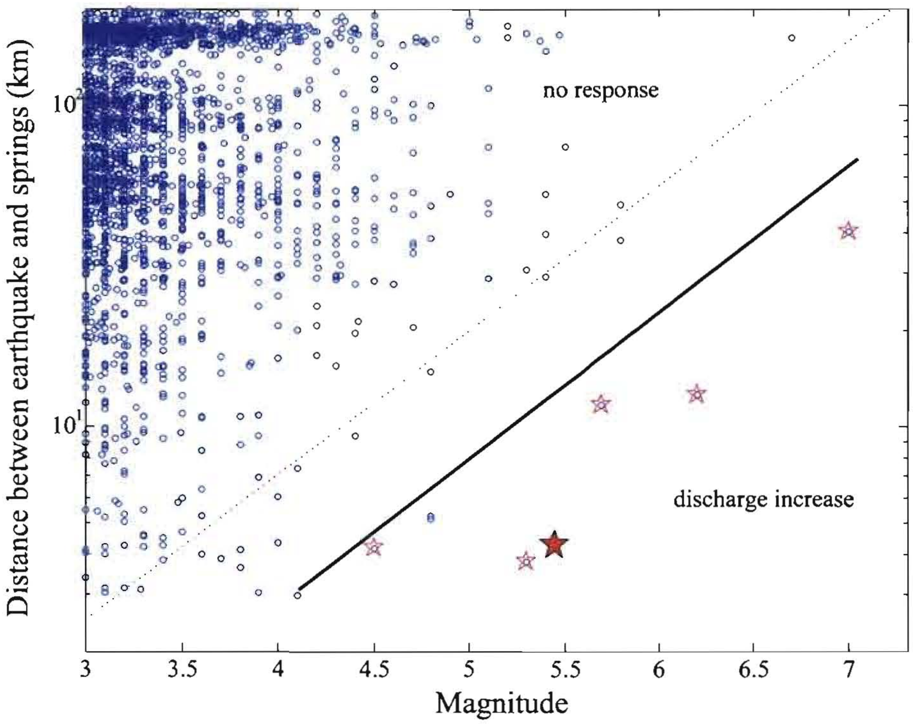

Fig. 7. Magnitude and distance from the springs of earthquakes that occurred during the period monitored: 1976-1991 by King et al. (1994), and 2003 - December 31, 2008 (Rowland et al., 2008 and present study). Red stars indicate earthquakes for which discharge increased; the filled-in star is the October 30, 2007 Alum Rock earthquake. Open blue circles are earthquakes for which there is no (documented) change in discharge. The sloping dashed line is an empirical magnitude-distance threshold for changes in streamflow based on a global compilation (Wang et al., 2006). The solid line is an empirically drawn line that separates earthquakes that caused discharge changes from those that did not.

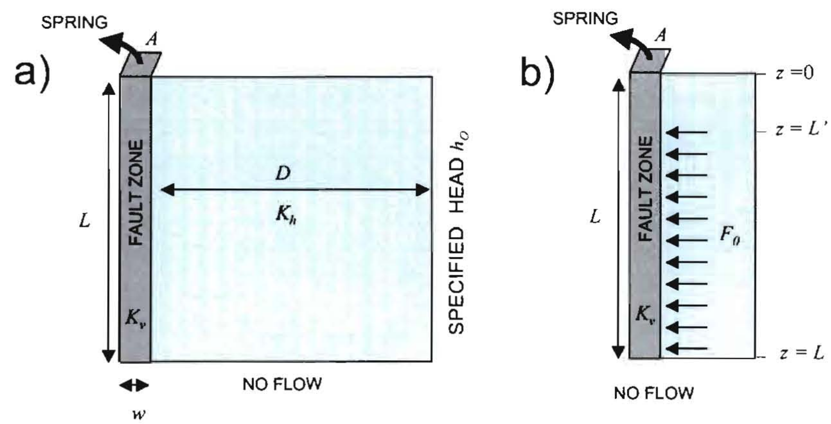

Fig. 8. Schematic illustration of conceptual models. a) Enhanced permeability model in which the vertical permeability of the fracture zone, K_v, changes after the earthquake. b) Increased head model in which an influx of fluid F causes the head in the fracture zone to increase and hence for discharge to increase.

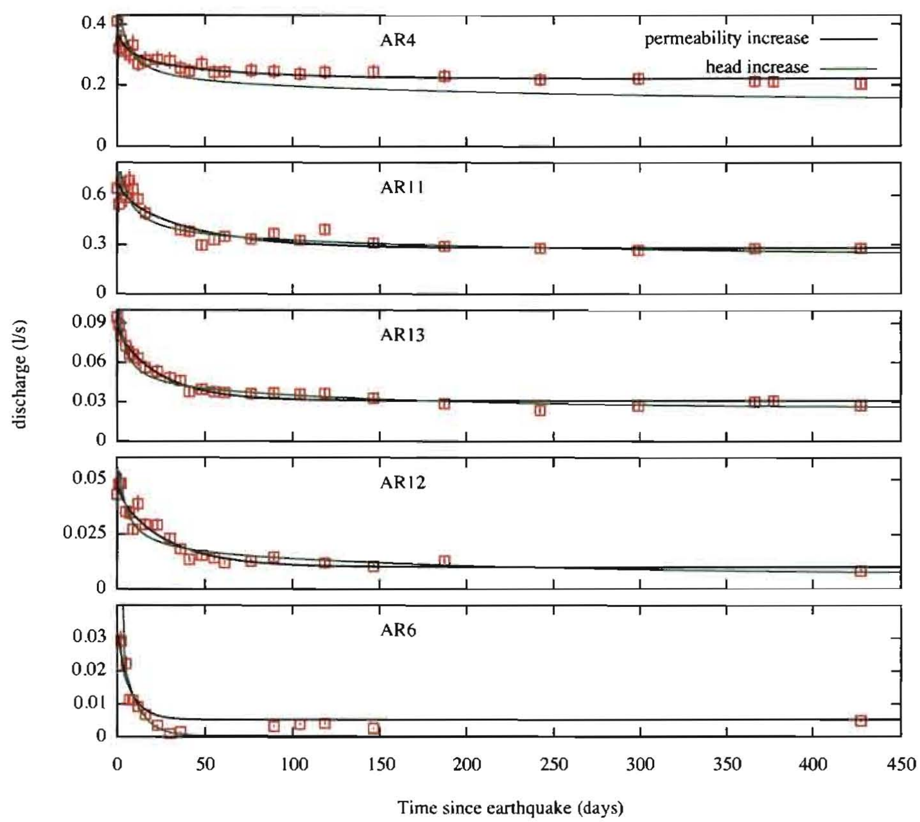

Fig. 9. Comparison of discharge measurements (symbols) with best fit models for the 5 springs for which reliable discharge measurements could be made. Black and blue curves are the enhanced permeability and increased head models, respectively, with models parameters listed in tables 3 and 4.

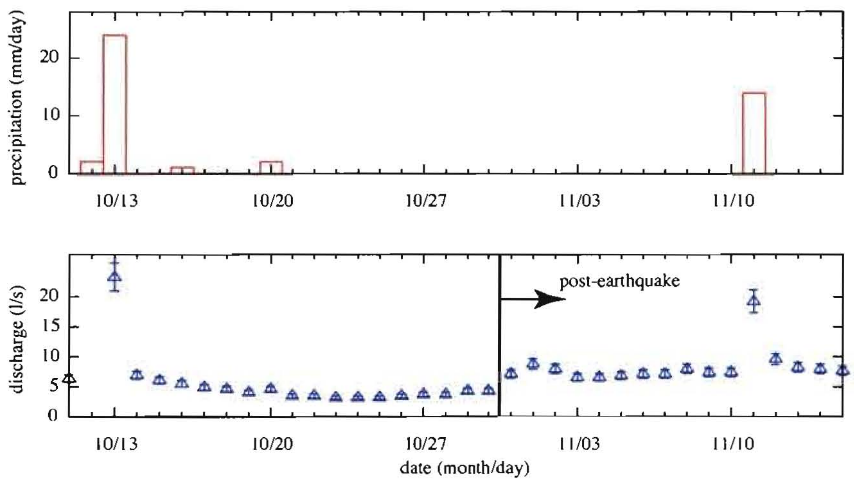

Fig. 10. Discharge in Penitencia Creek and precipitation before and after the October 30, 2007 Alum Rock earthquake. Discharge approximately doubled after the earthquake and remained elevated until precipitation on November 11 obscures any earthquake induced changes.

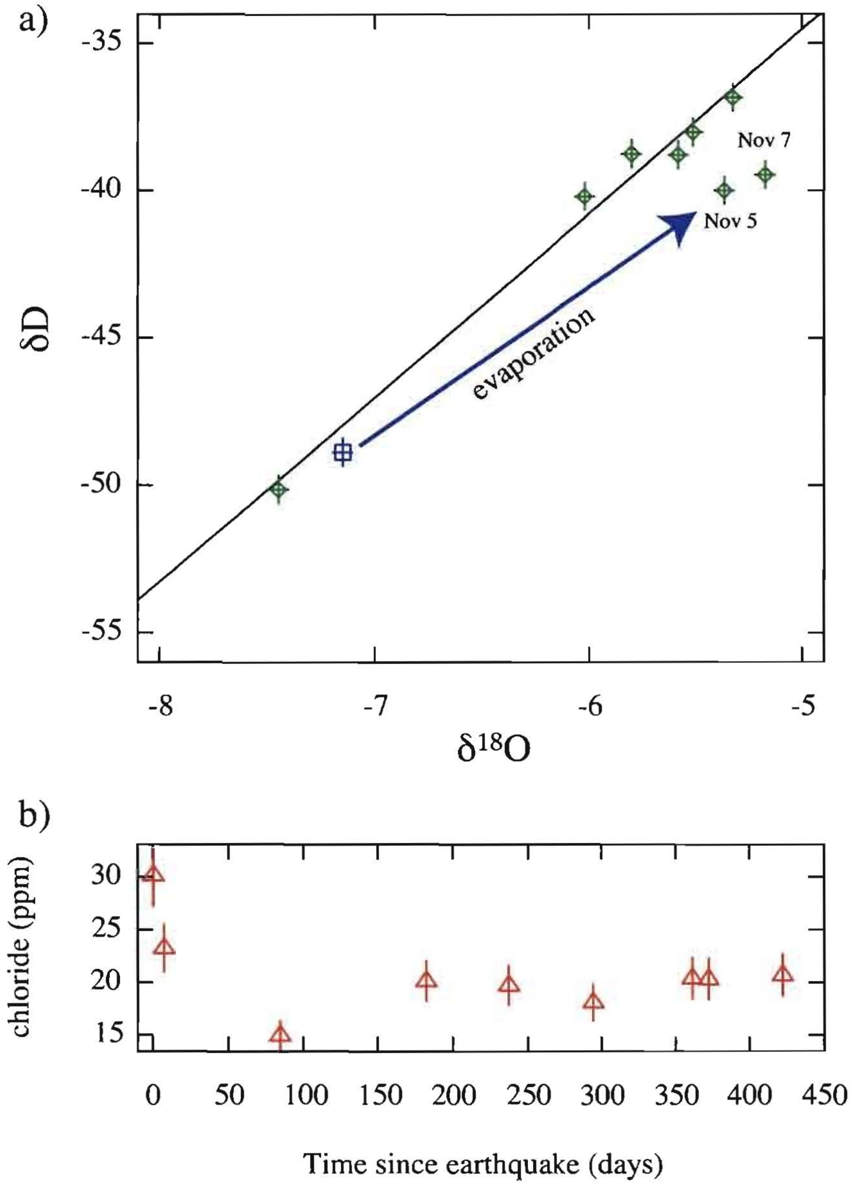

Fig. 11. a) Oxygen and hydrogen isotope composition of water collected from Penitencia Creek upstream of the springs and after the earthquake (green symbols). The black line is a best-fit to the measurements and has a slope of 6.3, lower than that of the global meteoric water line. The two outlier was the first sample collected after the earthquake on November 5 and 7. The blue symbol shows an estimate of water composition from which the November 5 sample could be derived by assuming 10% evaporation at 20°C and 50% humidity. b) Chloride time series showing that the high chloride concentration measured in creek water to date were in the first two weeks after the earthquake.

Table 1
Earthquakes followed by flow increases.

Date	Event	Magnitude	Epicentral distance	Volumetric strain[a]	Reference
4/18/1906?	San Francisco	7.8	70 km	D	Lawson (1908)?
4/24/1984	Morgan Hill	6.2	18 km	C	King et al. (1994)
3/31/1986	Mount Lewis	5.7	15 km	C	King et al. (1994)
6/13/1988	Alum Rock	5.3	8 km	C	King et al. (1994)
4/3/1989	Alum Rock	4.5	5 km	-	King et al. (1994)
10/18/1989	Loma Prieta	7.0	40 km	D	King et al. (1994)
10/30/2007	Alum Rock	5.5	4 km	-	This study

a. C, D and '-' indicate contraction, dilatation, or that the basin is close to a nodal plane in the strain, respectively.

Table 2
Model and expected changes at the springs.

Model	Prediction for the springs
Coseismic elastic strain	Temperature increase; larger fraction of deep water; correlation with sign of volumetric strain
Enhanced permeability	Temperature and composition changes will depend on where the changes occur; potential for permanent changes in flow and composition
Consolidation/liquefaction	Decreased temperature; larger fraction of shallow water; eventual return to pre-earthquake properties
Ruptured subsurface reservoirs and fault valves	Increased temperature; semi-permanent to permanent change in discharge and composition, with more deep water or new water component

Table 3
Model parameters for enhanced permeability model.

Spring	R	α (l/s)	T	ν (1/day)
AR4	3.0	0.14 ± 0.02	1.7 ± 0.2	0.0093 ± 0.0030
AR11	3.5	0.66 ± 0.18	0.70 ± 0.14	0.0039 ± 0.0018
AR13	3.6	0.19 ± 0.05	0.42 ± 0.06	0.0025 ± 0.0007
AR12	6.5	0.076 ± 0.047	0.37 ± 0.15	0.0018 ± 0.0016
AR6	50	0.012 ± 0.01	0.1[a]	0.00056 ± 0.00007

a. fixed to this value

Table 4
Model parameters for increased head model

Spring	Q_0 (l/s)	β (l/s)	Λ (1/day)
AR4	0.153	0.072 ± 0.007	0.0050 ± 0.0010
AR11	0.233	0.14 ± 0.01	0.0044 ± 0.0007
AR13	0.026	0.0205 ± 0.0007	0.0081 ± 0.0007
AR12	0.007	0.0127 ± 0.0006	0.0062 ± 0.0007
AR6	0	0.035 ± 0.004	0.115 ± 0.020

a. fixed to this value